Composite Structures 169 (2017) 173–179

Contents lists available at ScienceDirect

Composite Structures

journal homepage: www.elsevier.com/locate/compstruct

Terrestrial laser scanning technology for deformation monitoring and surface modeling of arch structures

Hao Yang [a,b], Mohammad Omidalizarandi [b], Xiangyang Xu [b,*], Ingo Neumann [b]

[a] Jiangsu University of Science and Technology, Zhenjiang City, Jiangsu Province, PR China
[b] Geodetic Institute, Faculty of Civil Engineering and Geodetic Science, Leibniz University Hanover, Hanover, Germany

ARTICLE INFO

Article history:
Received 10 September 2016
Revised 20 October 2016
Accepted 21 October 2016
Available online 22 October 2016

Keywords:
Terrestrial laser scanning
Deformation monitoring
Data extraction
Surface approximation

ABSTRACT

Terrestrial laser scanning (TLS) is capable to be a reliable deformation monitoring device with high-precision for concrete composite structures. Measurements based on TLS for an arch structure with monotonic loading is carried out. In this paper, comparison between original and optimized extraction of point clouds are presented. Surface approximation is implemented, where the vacant measurement area is also covered and the uncertainties of different-order surfaces are investigated. The results of surface approximation based on TLS measurement have certain relation with surface roughness of specimen, which will be eliminated by subtraction in deformation calculation.

1. Introduction

Terrestrial laser scanning (TLS) is capable to be a reliable deformation monitoring device with high-precision for composite structures. Since reinforced concrete (RC) and brick structures are regularly required to satisfy the high demands of comfort and security, they have been ubiquitous building materials and diffusely applied in various types of engineering structures. As a result, it is essential to monitor the deformation and assess safety of these structures against failure. And the prediction of the load-displacement behavior of the structures throughout the range of elastic and inelastic response is desirable [1–3].

1.1. Background

Measurement data can be acquired continuously or at specific time intervals during the lifetime of a structure and combined with damage detection routines. Various devices for acquiring 3D information have been applied in recent years and several studies have analysed the behaviour of these instruments [4–6]. Comparing with other devices for deformation measurement, one significant advantage of the TLS is that it has fewer requirements in experimental environment, and can easily be implemented with a simple experimental setup [7–8]. As terrestrial laser scanners have become more available, their applications have become more widespread, creating a demand for affordable, efficient and user-friendly devices [9].

Main principles of various TLS instruments are time-shifting, triangulation, and phase difference during the propagation of laser [10], where the currently used Z + F IMAGER 5006 is the third kind one. With the benefit of high-accurate measurement of distance and angles, 3D coordinates of grid points on object surface are obtained. Intensity of reflected laser, color, time, position, etc. can be additional data from TLS scanner. All the data are possible to be stored permanently and readable easily.

1.2. State of the art

Our work of deformation monitoring concerns two main parts: the first part is related to data extraction and segmentation, the second part is about surface approximation. Hybrid segmentation in both 3D object space and 3D image space (i.e. grayscale or RGB image) is proposed in [11]. Segmentation starts in object space by applying surface growing based on updating plane parameters and robust least squares plane fitting. Consequently, segmented results from object space is utilized to perform regional growing segmentation in image space to extract object boundaries more accurately.

Drawback of the proposed approach is that segmentation in the object and image spaces are not performed simultaneously. Thus, similarity of intensity values in image space will lead to under-segmentation. Superpixels algorithm avoids under-segmentation by reducing image complexity through pixel grouping [12]. It is

* Corresponding author.
E-mail address: xu@gih.uni-hannover.de (X. Xu).

http://dx.doi.org/10.1016/j.compstruct.2016.10.095
0263-8223/

based on voxel relations and takes advantages of spatial and color information of the object to produce over-segmentations results [11]. It is quite fast and has better performance in object boundary extraction comparing to other existing segmentation approaches. In this research, supervoxels segmentation benefits from both computed normal vectors of the point clouds and its reflectivity values as spatial and color information respectively.

Surface approximation from point clouds is popular in many fields, e.g. shape processing, rendering tasks [13], reverse engineering, etc. New attempt has been made in structural analysis with combination to physical models [14]. The salient benefits mainly lie in outlier removal, surface inspection, and piece wise instead of point wise record.

1.3. Motivation

In current experiment, an arch-shape construction made of concrete and brick material is investigated with multi-sensor system. The arch was set on the first floor while TLS scanner on the second floor for the purpose of the most scanning area of the specimen. After epoch measurements and data collection, point clouds extraction is carried out based on TLS data aiming at the isolation of top surface of the arch. Optimization of the extracted point clouds are processed thereafter by polygonal selection in Cloud Compare software.

These pre-steps offer point clouds exactly of the arch top surface and discarding the surrounding objects. Challenge in deformation analysis of the overall top surface of the arch is that vacant measurements is unavoidable in the experiment, for the reason that a series of steel beams on top of the specimen interrupted the views from the laser scanner. To solve this problem, parametric polynomial surface is proposed with elaborate discussion of uncertainties. Deformation referring to the complete arch area is computed based on that.

2. Experiment

The loading process is shown in Table 1, where each load interval is carried out with constant load speed. In between each load interval, there is a non-load period of 10 min, when the measurements are performed.

The emplacement of devices is shown in Fig. 1, where instruments are mainly classified for TLS Z + F IMAGER 5006 (the upper left), one Leica Laser tracker (the lower right) and one Nikon camera (the lower middle). Two extra cameras stood on both sides of Nikon camera, which are set by another institute to monitor the side surface of the arch.

The span of arch is 2 m and thickness is 10 mm. In this research, top surface of the arch is of utmost interest for deformation monitoring since it is under load pressure in 13 epochs and has significant deviations comparing to the other parts of object. In the future work, frontal part of object is taken into account for more precise deformation analysis.

Targets of TLS are set on stable platform on both sides for the possibility of data calibration. Some circular targets are attached to the stable platform on the left side of the arch and some are to the bottom of the arch (black circles in Fig. 2) for camera measurement. Utilizing camera would assist us to obtain feature points with high resolution since discrete feature point extraction is an advantage of camera [15]. In addition, 11 magnetic holders (red circles in Fig. 2) mounted on top of the arch, steel beams and surroundings are measured by laser tracker, which is an accurate sensor system with maximum permissible error of 15 μm + 6 μm/m, which provides this possibility to compare with processed TLS data in the future.

Table 1
Load steps of the arch experiment.

Steps	Load range	Load speed
1	0–12 mm	0.002 mm/s
2	12–14 mm	0.003 mm/s
3	14–20 mm	0.004 mm/s

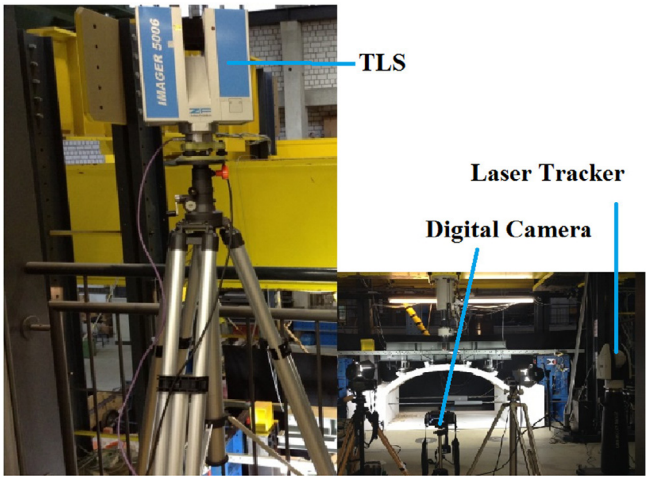

Fig. 1. The experiment set up.

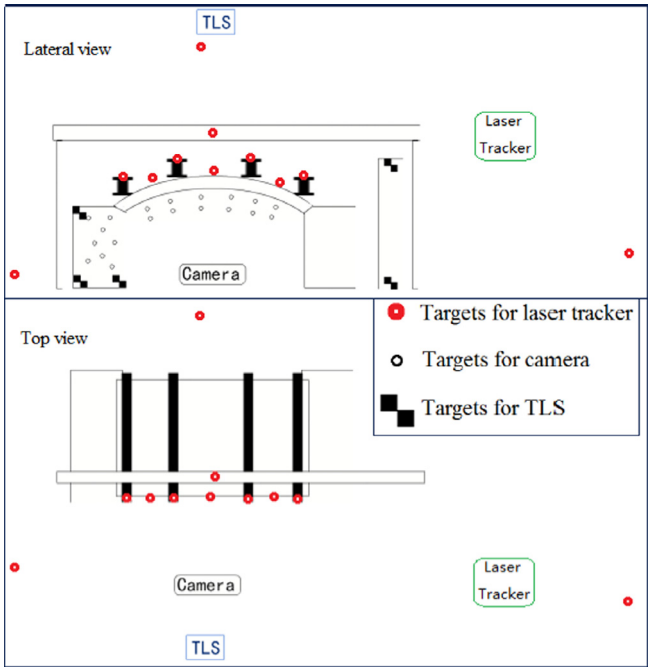

Fig. 2. Sketch of instruments in the measurement.

3. Data extraction

The arch is occluded with some other objects (e.g. beams and so on) and needs to be separated that enables us to perform surface approximation more accurately. Work flow of data extraction is presented in Fig. 3.

With raw TLS point clouds data, reflectance image is generated from intensity value. Thresholding and filtering is performed

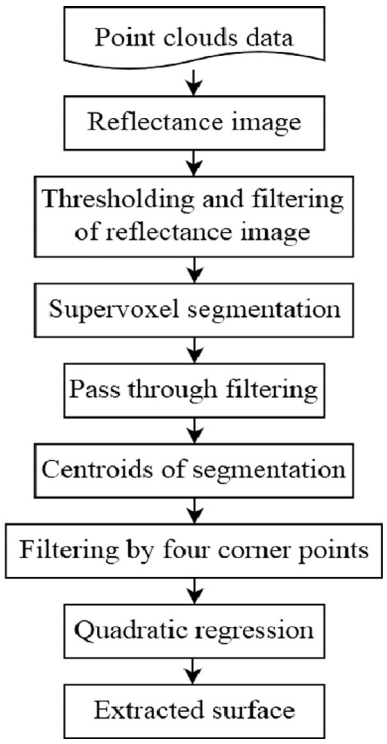

Fig. 3. Work flow of data extration.

thereafter to remove the surrounding objects of the arch top surface. Then supervoxel segmentation is carried out, where for each segmentation, its centroid is obtained. Filtering and quadratic regression are conducted to obtain the point clouds of top surface of the arch.

The extraction of point clouds corresponding to the top surface is carried out based on laser intensity data of TLS measurement. Scheme of entire monitored object which colorized with reflectivity values using Z + F Laser Control software is depicted in Fig. 4a. Reflectance image can be generated by mean of scanning matrix approach for which each 3D point is assigned to one pixel based on scan resolution [16]. Scheme of generated reflectance image is represented in Fig. 4b. As can be seen in this Figure, occluded objects such as beams on top of the arc-shape object are darker with respect to the arc-shape part and can be discarded by means of thresholding and morphological opening and closing filters (see Fig. 4b).

In the next step, point clouds are divided into a number of supervoxel clusters using Point Cloud Library (PCL). Voxel Cloud Connectivity Segmentation (VCCS) is an especial type of superpixel segmentation approach which aims to produce volumetric oversegmentations of 3D point cloud data which is known as supervoxels [11].

As can be seen from Fig. 4c, supervoxel segmentations of monitored object in addition to the normal vector of each segment with small line representing its direction are depicted. Furthermore, Pass Through filter of the PCL library is applied to discard those 3D point cloud data below pre-defined threshold in the z-axis direction. In the next step, centroids of the segmented point clouds from segmentation step is computed and those center points that are within four corner points of the arc-shape object are selected.

Thereafter, selected center points are projected in the vertical plane and quadratic regression is applied. As can be seen from Fig. 4d, those center points above pre-defined threshold from estimated polynomial are discarded throughout adjustment procedure as outliers. Final extracted arc-shape object is illustrated, where the gap between each point cloud patch is caused by shadows of other objects, e.g. steel beams, corner cubes, etc.

4. Analysis

According to the arch top surface approximation presented in Fig. 8, the approximation standard deviation between the point clouds and the surface is 2.69 mm, which is shown in Table 2. Matlab and Software and Cloud Compare (V2.7.0) are together used to

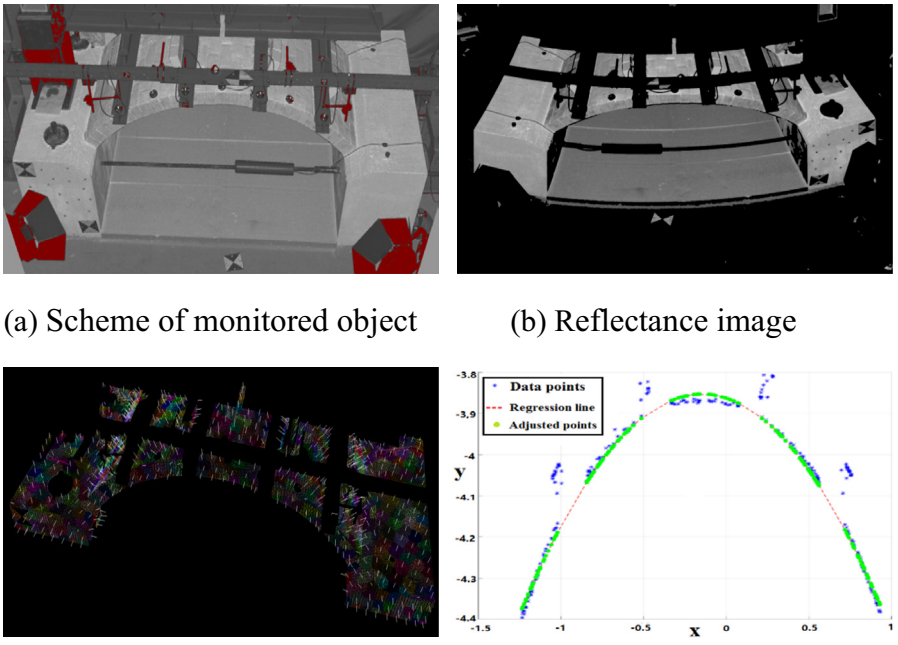

(a) Scheme of monitored object (b) Reflectance image

(c) Supevoxel segmentation (d) Quadratic polynomial regression

Fig. 4. Results of data extracted processing.

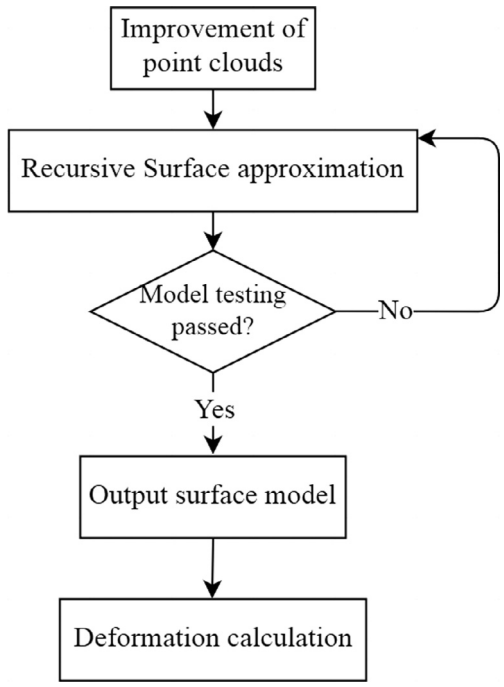

Fig. 5. Process of deformation achievement.

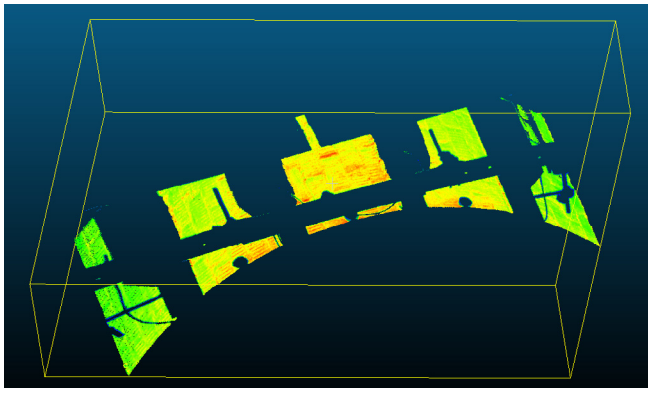

Fig. 6. Three dimensional point clouds in cloud compare.

improve the extraction in order to reduce the standard deviation which is defined as Eq. (1).

$$\sigma = \sqrt{\frac{1}{N}\sum_{i=1}^{N}(x_i-\mu)^2}; \quad \mu = \frac{1}{N}\sum_{1}^{N}x_i; \quad i = 1,2\ldots \tag{1}$$

Here X takes random values from a finite data set $X_1, X_2, X_3 \ldots, X_N$, with each value having the same probability. Improvement of extracted point clouds is followed by surface modeling and deformation calculation, which are presented in Fig. 5.

During this process, different order approximated surfaces of improved point clouds are checked by model testing. If the surface doesn't pass model testing, the order of the surface is increased till the passing of model testing. Then the surface model is output and deformation of the arch is calculated by substraction of two epoch surfaces.

Extracted point clouds with increased density are transferred to text file format by MATLAB as point array and then input into Cloud Compare. Polygon selection is performed from the lateral side of the arch. The improved point clouds in Cloud Compare is shown in Fig. 6.

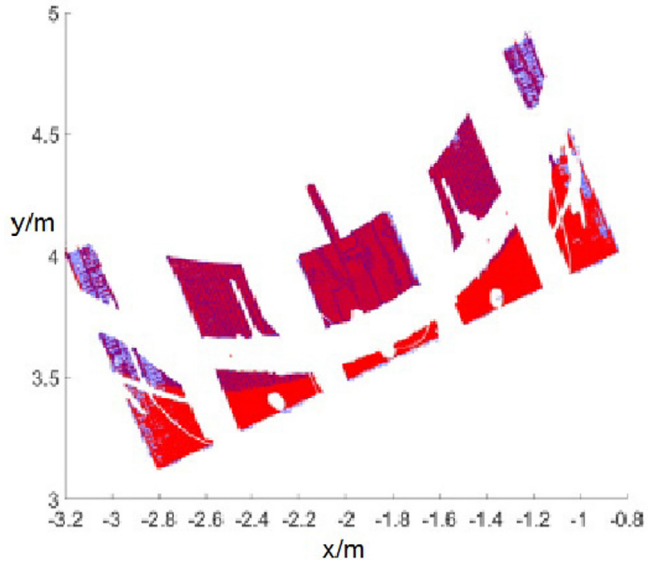

Fig. 7. The comparison of segmentation extractions.

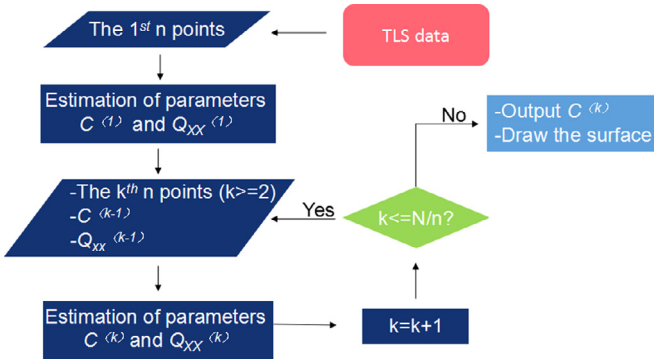

Fig. 8. Process of recursive polynomial approximation.

Table 2
The optimization of surface approximation.

Approximation based	Standard deviation
Original extraction	2.69 mm
Optimized extraction	2.07 mm

The corrected point clouds is compared with the original extraction in Fig. 4, where the red parts refer to correction, the blue parts refer to the original extraction.

According to Fig. 7, it can be observed that they overlap each other in most part, but have some deviation in the areas near the edge. And the surface roughness of concrete also raises the standard deviation of surface polynomial approximation which indicates that it is more appropriate to calculate deformation of epoch data with polynomial than with the method of B-spline.

The process of recursive polynomial surface approximation is presented in Fig. 8. Firstly, the first n points is input, where n can be 1000 according to the amount of total point number.

$$\hat{\mathbf{C}} = (\mathbf{M}^T\mathbf{M}^{-1})\mathbf{M}^T\mathbf{Z}; \quad \mathbf{Q}_{\hat{x}\hat{x}} = (\mathbf{M}^T\mathbf{M}^{-1}) \tag{2}$$

Secondly, coefficient matrix $\mathbf{C}$ and cofactor $\mathbf{Q}_{xx}$ of the first n points is computed after Eq. (2), where $\mathbf{M}$ is the design matrix which is constructed based on mathematical function of the surface, Z is observation, here it is Z coordinates of each point.

$$\hat{\mathbf{C}}^{(k)} = \hat{\mathbf{C}}^{(k-1)} + \mathbf{Q}_{\hat{x}\hat{x}}^{(k-1)}\mathbf{M}^T(\mathbf{M}\mathbf{Q}_{\hat{x}\hat{x}}^{(k-1)}\mathbf{M}^T)^{-1}(\mathbf{z} - \mathbf{M}\hat{\mathbf{C}}^{(k-1)}) \quad (3)$$

$$\mathbf{Q}_{\hat{x}\hat{x}}^{(k)} = \mathbf{Q}_{\hat{x}\hat{x}}^{(k-1)} - \mathbf{Q}_{\hat{x}\hat{x}}^{(k-1)}\mathbf{M}^T(\mathbf{M}\mathbf{Q}_{\hat{x}\hat{x}}^{(k-1)}\mathbf{M}^T)^{-1}\mathbf{M}\mathbf{Q}_{\hat{x}\hat{x}}^{(k-1)}$$

Thirdly, recursive calculation is performed starting from the next n points after Eq. (3), where $\mathbf{C}^{(k)}$ and $\mathbf{Q}_{\hat{x}\hat{x}}^{(k)}$ mean the coefficient and cofactor of the k^{th} recursion. If all the points are computed, the surface coefficient matrix is output and surface approximation finished, otherwise, the recursion steps on.

4.1. Optimization

The measurement accuracy and resolution of TLS are much higher than traditional measuring instruments, therefore, it has potential capability to be one of the most high precision monitoring devices for deformation monitoring. However, the rough standard deviation of surface approximation decrease the advantage of TLS measurement, thence optimization is required.

Fig. 9 is 3D view of the arch which presents both point clouds and surface approximation. The measured point clouds are marked in blue and the approximated surface is drawn with color bar. We can observe from Fig. 9 that the polynomial surface agrees well with the point clouds in the longitudinal deformation displacement which corresponds to the value of Z coordinate. However, the polynomial surface in the top and two ends separate from their point clouds in the opposite of Z axis direction. That is because the polynomial method tends to approximate surface whose curvature doesn't change sharply.

Surface approximation is made based on the point clouds. The benefits of surface approximation are that the point clouds are averaged and forms a surface model. It makes great sense because the deformation of arbitrary point is available based on the scanned data of scattered points. Gauss Markov model is adopted to compute the coefficients of polynomial function. Computation details of surface approximation can be found in [18].

Surface quality is investigated in detail, after the surface approximation. Deviation of each point to the approximated surface is computed. It can be observed in figure that the deviation of points to second-order polynomial surface mainly distributes in the range [−20, 40] mm. To decrease the deviation and increase the surface fitness, higher order polynomial surfaces are considered.

Model testing is employed to find a best polynomial surface. The order of the polynomial surface changes from 2 to the higher.

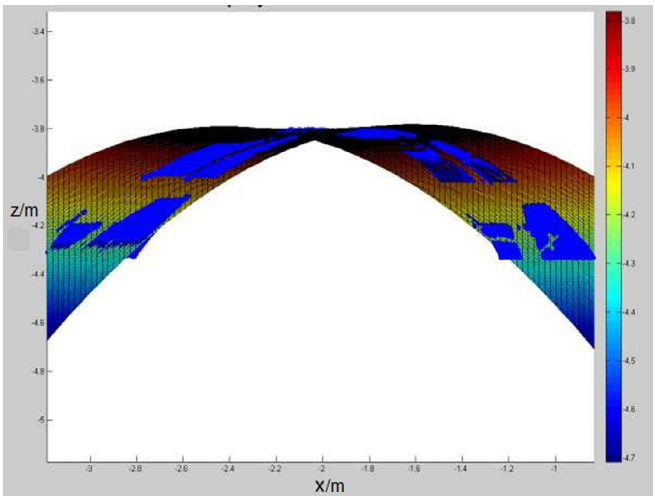

Fig. 9. Surface approximation.

Each order polynomial surface is compared with the higher order polynomial surface. Finally, the fourth-order polynomial surface is chosen as the best-fit polynomial surface with a standard deviation of 2.07 mm. It is consistent with Fig. 10, where the fourth-order polynomial surface has a deviation range much more concentrated compared with the other two. The distribution in figure is fractured due to the reason that the corresponding part of the arch is sheltered by steel beam and blank occurs in the point clouds.

The surface difference is calculated by the comparison of surfaces between epoch one and epoch two. According to the Fig. 11, we can observed that the surface difference fitted by the polynomial approximation, are symmetric in the diagonal direction, but a gradient appears in the anti-diagonal direction, because in this measurement TLS is not aligned to the arch concrete but is inclined. The surface differences are symmetrical only in the direction of diagonal which means that the arch is twisted when the loads are increasing.

5. Results

The standard deviation of the optimal polynomial surface is 2 mm. This can be due to several reasons.

(i) Material reasons. The arch in the experiment is made of brick. There is inevitable depression in the connection of bricks, which means the arch shape is not absolutely smooth. What's more, the brick material itself does not reflect the laser evenly, and this effect should be more obvious for brick than concrete painted with lime [paper IEEE sensors].

(ii) Measurement reasons. On the one hand, range noise of TLS commonly exists in measurements, e.g. when measuring white object with a 100% reflectivity, the range noise at 10 m distance is 0.7 mm according to the instruction sheet of Z + F IMAGER 5006. On the other hand, the arch-shape point clouds are extracted by reflectance information of TLS, for which uncertainties increase near the shadow of the steel beam.

(iii) Calculation reasons. The point cloud segmentation is obtained through quadratic function. However, the noise of the extracted point clouds still exist through this way, which brings a large uncertainty to the fitted surface. The noise should be eliminated and error should be controlled.

The comparison between original and optimized extraction is presented in Fig. 12, where the blue parts correspond to the original extraction and the red parts refer to optimized.

It can be observed that the original extraction is more disarray and fluctuant. The noise-likely point clouds increase the standard deviation of surface approximation and influence approximation consequent.

The surface approximation of original extraction has a standard deviation of 2.69 mm, while the corresponding value of the corrected point clouds is 2.07 mm (see Table 2). One reason is that the corrected point clouds decrease the noise of the original extraction, which can be observed from Fig. 11. In future experiment, through the benefit of multi-sensor measurement, such as combining laser tracker and high accuracy cameras, the standard deviation of surface approximation can be reduced further.

Possible method can be robust approximation, which contains the following points:

(i) compare for every point the orthogonal distance to the fitted surface and sigma.

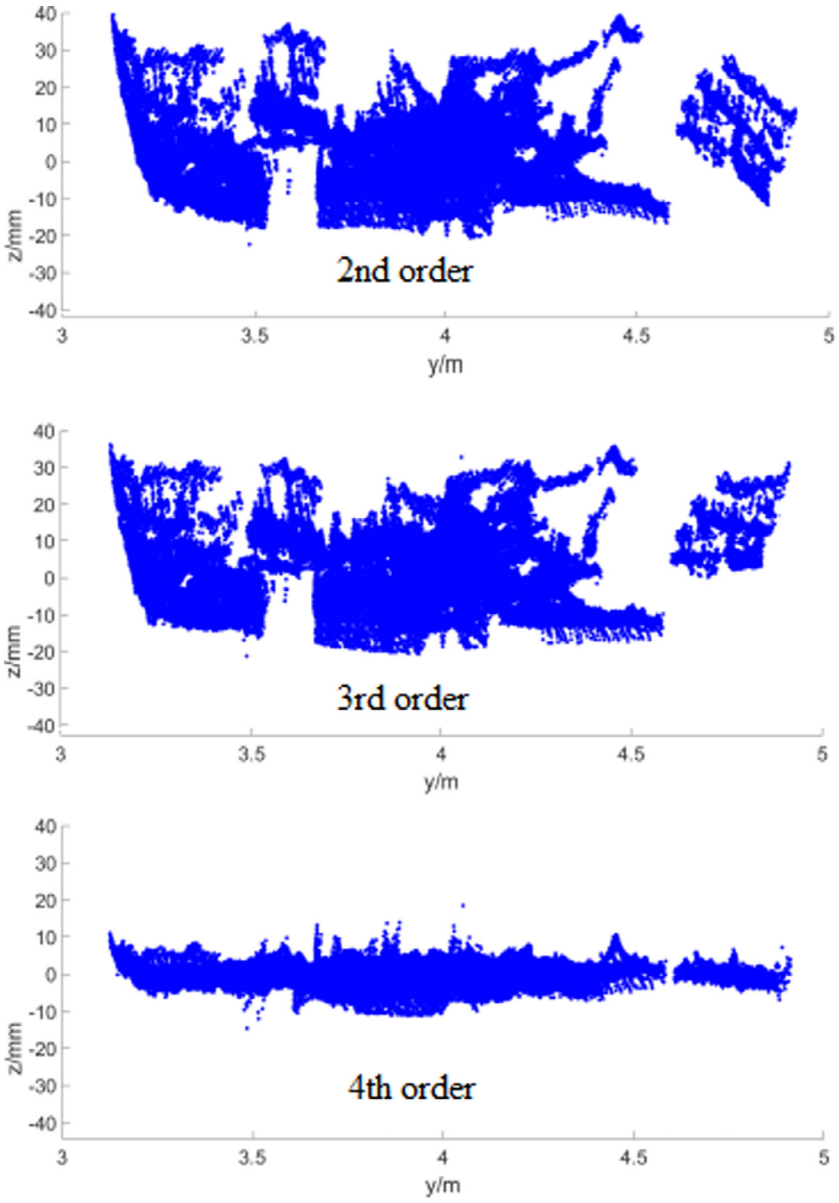

Fig. 10. Deviation of point clouds to approximated surfaces.

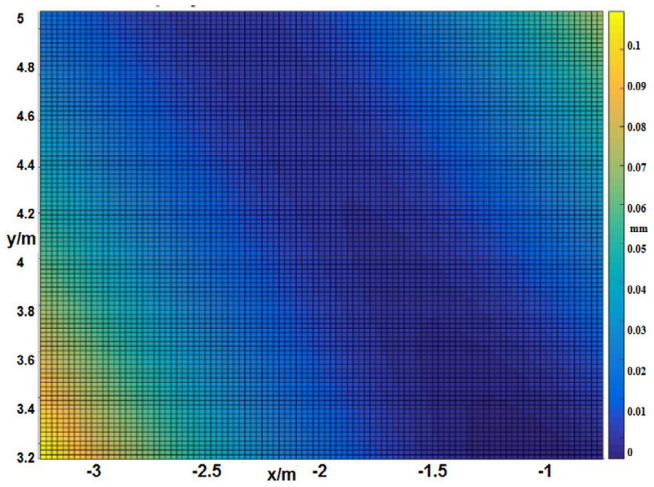

Fig. 11. The surface difference.

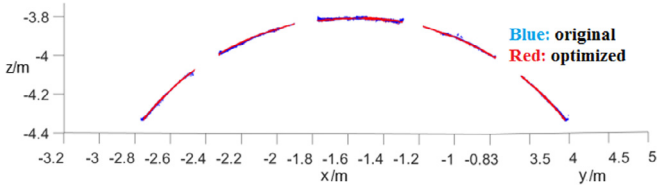

Fig. 12. The comparison of original and optimized extraction.

(ii) if the distance is larger, the weight of the point to the surface is decreased, e.g. from 1 to 0.01. The decreased value can be sigma/d or defined in other ways.
(iii) after every weighted point, the surface is calculated iteratively, till the sigma is accepted, e.g. less than 1 mm.

6. Conclusion

In this experiment, an arch structures under monotonic loads measurement based on terrestrial laser scanning technology is car-

ried out. Thirteen epochs are recorded and the information is collected as point clouds which are imported by Z + F Laser Control software. The point clouds are extracted by the PLC and corrected by MATLAB program.

In this paper, the comparison between original and optimized extraction is presented where the standard deviation corresponds to 2.69 and 2.07. The result surface approximation based on TLS measurement have certain relation with the surface roughness of concrete. By means of optimizing the point clouds extraction, standard deviation of surface approximation will be reduced by 23% and approximation consequent can be improved.

The achieved deformation surface is capable to be applied in analysing the deformation between different epochs at arbitrary point on top surface of the arch construction, especially within the occluded area where it is hard to measure with instruments. At the moment, the deformations are computed point wise, what means that the difference of the two surfaces in each epoch is calculated by the difference of two points that lie on these two surfaces. This leads to a dense point wise representation of the deformation. This calculation of a real deformation surface is sufficiently accurate without any significant approximation error. For the future, the goal is to describe the deformation by a real continuous mathematical surface. This should be relatively easy for polynomial surfaces but is a challenging task for more complex surfaces.

It is also necessary and important to mentioned that this proposed strategy could be used, e.g., within the minimal mass reinforcement strategy of curved masonry structures proposed [17,18]. Such a strategy which makes indeed use of points clouds to describe the geometry of the structure.

Conflicts of interest

The authors declare no conflict of interest.

Acknowledgments

The authors of this paper are supported by Deutsche Forschungsgemeinschaft and Open Access Publishing Fund of Leibniz Universität Hannover. The authors also would like to acknowledge the support of Natural Science Foundation of Jiangsu Province (No: BK20160558).

References

[1] Qapo Michael, Dirar Samir, Jemaa Yaser. Finite element parametric study of reinforced concrete beams shear-strengthened with embedded FRP bars. Compos Struct 2016;149:93–105.
[2] Schefer RW. Three-dimensional structure of lifted, turbulent-jet flames. Combust Sci Technol 1997:371–84.
[3] Hult J, Meier U, Meier W, Harvey A, Kaminski CF. Experimental analysis of local flame extinction in a turbulent jet diffusion flame by high repetition 2D laser techniques and multi-scalar measurements. Proc Combust Inst 2005:701–9.
[4] Steen Magnussen S, Wulder A. Post-fire canopy height recovery in Canada's Boreal forests using airborne laser scanner (ALS). Remote Sens 2012;4:1600–16.
[5] Straub C, Koch B. Estimating single tree stem volume of pinus sylvestris using airborne laser scanner and multispectral line scanner data. Remote Sens 2011;3:929–44.
[6] Park JH, Shim J, Lee DY. A compact vertical scanner for atomic force microscopes. Sensors 2010;10:10673–82.
[7] Maas H-G, Bienert A, Scheller S, Keane E. Automatic forest inventory parameter determination from terrestrial laser scanner data. Int J Remote Sensing 2008;29(5):1579–93.
[8] Olsen MJ, Kuester F, Chang BJ, Hutchinson TC. Terrestrial laser scanning-based structural damage assessment. J Comput Civ Eng 2010:2464–72.
[9] Yang H, Xu X, Neumann I. Laser scanning-based updating of a finite element model for structural health monitoring. IEEE Sensor 2016:2100–4.
[10] Vosselman G, Maas H. Airborne and terrestrial laser scanning. Scotland, UK: Whittles Publishing; 2010. p. 12–53.
[11] Papon J, Abramov A, Schoeler M, Worgotter F. Voxel cloud connectivity segmentation-supervoxels for point clouds. In: Proceedings of the IEEE conference on computer vision and pattern recognition; 2013. p. 2027–2034.
[12] Ren X, Malik J. Learning a classification model for segmentation. In: Proceedings ninth IEEE international conference on computer vision; 2003. p. 10–7.
[13] Anders Adamson, Marc Alexa. Approximating and Intersecting Surfaces from Points, Eurographics Symposium on Geometry Processing; 2003.
[14] Yang H, Xu X, Neumann I. The benefit of 3D laser scanning technology in the generation and calibration of FEM models for health assessment of concrete structures. Sensors 2014;14(2014):21889–904.
[15] Omidalizarandi M, Neumann I. Comparison of target- and mutual information based calibration of terrestrial laser scanner and digital camera for deformation monitoring. Int Arch Photogramm Remote Sensing Spatial Inf Sci 2015;40(1):559.
[16] Meierhold N, Spehr M, Schilling A, Gumhold S, Maas HG. Automatic feature matching between digital images and 2D representations of a 3D laser scanner point cloud. Int Arch Photogramm Remote Sens Spatial Inf Sci 2010;38:446–51.
[17] Fabbrocino F, Farina I, Berardi VP, Ferreira AJM, Fraternali F. On the thrust surface of unreinforced and FRP-/FRCM-reinforced masonry domes. Compos Part B Eng 2015;83:297–305.
[18] Fraternali F, Carpentieri G, Modano M, Fabbrocino F, Skelton RE. A tensegrity approach to the optimal reinforcement of masonry domes and vaults through fiber-reinforced composite materials. Compos Struct 2015;134:247–54.